

Hardware efficient quantum simulation of non-abelian gauge theories with qudits on Rydberg platforms

Daniel González-Cuadra,^{1,2,*} Torsten V. Zache,^{1,2,*} Jose Carrasco,¹ Barbara Kraus,¹ and Peter Zoller^{1,2}

¹*Institute for Theoretical Physics, University of Innsbruck, 6020 Innsbruck, Austria*

²*Institute for Quantum Optics and Quantum Information of the Austrian Academy of Sciences, 6020 Innsbruck, Austria*

Non-abelian gauge theories underlie our understanding of fundamental forces in nature, and developing tailored quantum hardware and algorithms to simulate them is an outstanding challenge in the rapidly evolving field of quantum simulation. Here we take an approach where gauge fields, discretized in spacetime, are represented by qudits and are time-evolved in Trotter steps with multi-qudit quantum gates. This maps naturally and hardware-efficiently to an architecture based on Rydberg tweezer arrays, where long-lived internal atomic states represent qudits, and the required quantum gates are performed as error-tolerant holonomic operations supported by a Rydberg blockade mechanism. We illustrate our proposal for a minimal digitization of SU(2) gauge fields.

Introduction.— Quantum field theories form the backbone of the Standard Model of particle physics, where quantized gauge fields mediate the interactions between fundamental particles [1]. Lattice gauge theories (LGTs), where fields are discretized on a space-time lattice [2], provide a convenient framework to study non-perturbative high-energy phenomena, and have been extensively used to extract numerous experimentally relevant predictions [3]. Despite this success, standard approaches based on Monte Carlo methods are severely limited by the sign problem [4], preventing the study of real-time gauge theory dynamics, among other drawbacks. The latter are essential to analyze experimental results in heavy-ion colliders, where open problems in particle physics are currently being addressed [5, 6], including the search of new physics beyond the Standard Model.

In the recent years, quantum simulators (QS) [7] have emerged as a promising pathway to circumvent these problems [8–13], leading to several experimental demonstrations where simple LGTs were investigated using digital, analog and variational methods [14–20]. For digital QS [21], in particular, different schemes have been proposed to address high-dimensional non-abelian gauge theories using different platforms, including trapped ions [22–24], ultracold atoms [25–29], superconducting circuits [30–32] and cavities [33]. Despite their higher flexibility to simulate complex many-body Hamiltonians compared to the analog approach, crucial in particular for non-abelian theories, a full digital quantum simulation requires access to gate-based quantum computers, which are currently restricted to Noisy Intermediate Scale Quantum (NISQ) devices [34], limited in qubit number and circuit depths. Although an impressive effort is currently taking place to reduce the computational complexity using improved quantum software [35–49], simulating relevant LGTs in the NISQ era must be

complemented by the development of efficient quantum hardware tailored to the specific algorithmic demands.

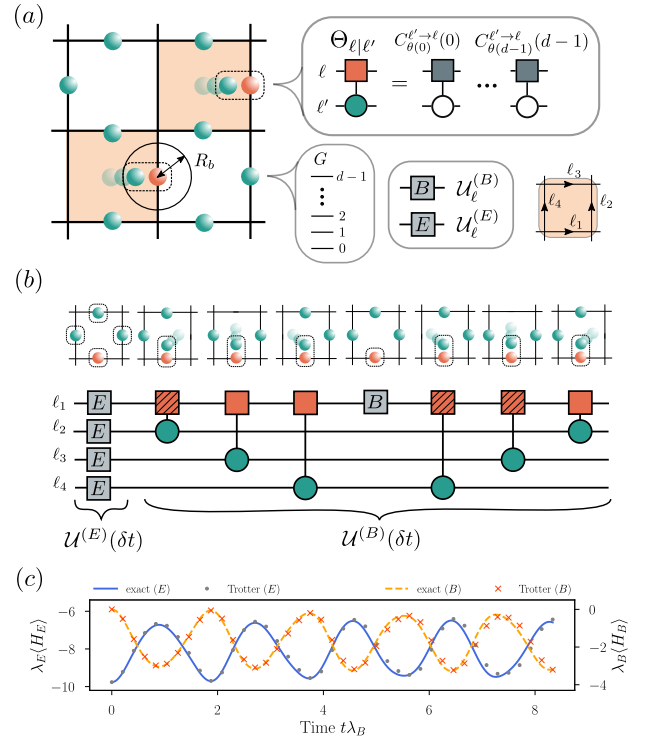


FIG. 1. Gauge field dynamics on a qudit quantum simulator: (a) Our proposal employs Rydberg atoms trapped in optical tweezers, arranged on the links ℓ of a hypercubic lattice. Each qudit encodes a qudit number d of internal levels, where single-qudit gates are realized holonomically. To implement the entangling two-qudit gate $\Theta_{\ell|\ell'}$, tweezers are rearranged to bring pairs of atoms within the Rydberg blockade radius R_b . (b) First order decomposition of a Trotter step, including the four-qudit plaquette interaction, into the native atomic gates $U_{\ell}^{(E/B)}$ and $\Theta_{\ell|\ell'}$ (see main text). (c) Trotterized quench dynamics of a non-abelian Q_8 LGT on a single plaquette for $\lambda_E/\lambda_B = 2.88$.

* These authors contributed equally.

cited to Rydberg states [50–56] (Fig. 1). We co-design the platform to match the requirements to digitally simulate real-time dynamics of non-abelian gauge theories in a hardware-efficient manner, showing a considerable reduction of experimental resources. In particular, we employ multi-level atoms to encode large gauge-field Hilbert spaces using long-lived qudits [57, 58], providing a reduction in complexity compared to qubit-based approaches [59]. Employing a Rydberg blockade mechanism [51, 52, 60], we develop a native set of holonomic gates [61–65], robust against decoherence, that allows to efficiently simulate the time evolution under a general LGT Hamiltonian. Although qudit-based quantum simulators can also be implemented with other platforms such as trapped ions [66] or photonic circuits [67], multi-dimensional tweezer arrays, both dynamically reconfigurable and locally addressable [53, 56, 68–71], satisfy the scalability requirements necessary to properly address the continuum limit of LGTs.

We emphasize that all the required ingredients of our proposal are available in current experimental platforms [53], as we illustrate for the simplest non-trivial digitization of the $SU(2)$ gauge theory. In this context, we also briefly comment on how to verify the outcome of the quantum simulation, establishing a clear roadmap to tackle open questions in particle physics using scalable near-term quantum devices.

Qudit quantum computing with Rydberg atoms.

Atomic systems offer the possibility to encode quantum information in internal states. Here, we go beyond the paradigmatic model of a two-level atomic qubit and consider a collection of N multi-level atoms in state-independent optical traps. For every single atom, we propose to encode a *qudit* with corresponding Hilbert space spanned by $|j\rangle$, $j = 0, \dots, d-1$ in d long-lived hyperfine ground states $|F, m_F\rangle$, where large hyperfine manifolds can be accessed e.g. using Erbium [72] or Holmium [73, 74]. In a qubit-based approach, an equivalent Hilbert space of dimension d^N requires control over $N \log_2(d)$ instead of only N atoms as in our case. We anticipate this saving of physical resources to be crucial for efficient near-future applications in the NISQ era.

The quantum information stored in each atomic qudit can be efficiently manipulated using holonomic operations [61], where arbitrary single-qudit gates $U \in SU(d)$ can be synthesized via an appropriate sequence of laser pulses, with time-dependent Rabi frequencies $\Omega(t)$. To see this, we first decompose U into a product of at most $d(d-1)/2$ unitaries acting non-trivially only on two atomic levels (i, j) [75], and subsequently realize the two-level unitaries via at most three rotations around the x or y axis, denoted by $R_{x(y)}^{(i,j)}(\varphi)$, respectively, utilizing an auxiliary state $|e\rangle$ [see the Supplemental Material (SM) [76] for details]. The total time required to implement a general single-qudit gate is upper bounded by $3d(d-1)T/2$, where T is the duration of a laser pulse, estimated below for realistic experimental parameters. We note that the explicit implementation of this scheme

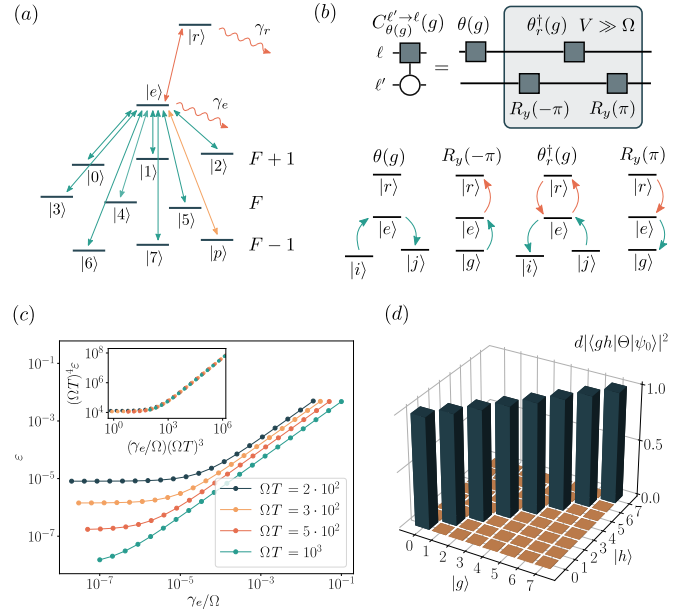


FIG. 2. **Qudit encoding and native gates:** (a) Atomic level structure designed to serve as a G -register for Q_s , where the $d = 8$ group basis elements are encoded into different hyperfine manifolds. Single and two-qudit gates are performed holonomically using the auxiliary ground-state level $|p\rangle$ and excited states $|e\rangle$ and $|r\rangle$ (Rydberg state), with corresponding decay rates γ_e/γ_r . (b) Controlled-permutation gate $C_{\theta(g)}^{\ell\ell' \rightarrow \ell}(g)$ as a sequence of four single qudit-gates in the blockade regime. (c) Infidelity ϵ for the single-qudit magnetic gate $\mathcal{U}_\ell^{(B)}$ for a Trotter time step $\delta t = 0.1$ as a function of γ_e/Ω and ΩT . Inset: The error follows a simple scaling relation, consisting of a power-law and a saturation regime. (d) Maximally-entangled state obtained after applying the $\Theta_{\ell|\ell'}$ to $|\Psi_0\rangle$ for $\Omega T = 300$ and $V/\Omega = 5$, obtaining a state fidelity of 99.93%.

should be guided by the constraints imposed by atomic selection rules, see Fig. 2(a) for an example with $d = 8$.

We now come to the main challenge of qudit quantum computing and introduce a new protocol for a general class of controlled-unitary operation, $C_U(j_0) = U \otimes |j_0\rangle\langle j_0| + \mathbb{1} \otimes (\mathbb{1} - |j_0\rangle\langle j_0|)$ with $j_0 \in \{0, \dots, d-1\}$. Our proposal is based on the Rydberg blockade mechanism [51, 52, 60], which prohibits the simultaneous excitation of two atoms to the Rydberg state $|r\rangle$ when their distance R is below the blockade radius, R_b , set by the large Rydberg interaction $V \sim 1/R^6 \gg \Omega$. This idea gives rise to the following protocol. First, bring the control and target atoms within range $R < R_b$ and apply the unitary U on target (as outlined above). Now excite the control qudit from $|j_0\rangle$ to the Rydberg state $|r\rangle$ using $S_{(j_0,r)} \equiv R_y^{(j_0,r)}(\pi)$, and subsequently realize U^\dagger on the target by decomposing every two-level rotation as $R_{x/y}^{(i,j)}(\varphi) = S_{(i,r)}^\dagger R_{x/y}^{(j,r)}(\varphi) S_{(i,r)}$ [Fig. (2)(b)]. To emphasize the involvement of the Rydberg state we denote this gate by U_r^\dagger . Finally, applying $S_{j_0,r}^\dagger$ to the control qudit maps the state $|r\rangle$ back to $|j_0\rangle$. Due to the Rydberg

blockade, which projects onto the subspace orthogonal to the state $|rr\rangle$ (both atoms in the Rydberg state), this protocol realizes the operator

$$(\mathbb{1} \otimes S_{(j_0,r)}^\dagger) [\mathcal{P}(U_r^\dagger \otimes \mathbb{1})\mathcal{P}] (\mathbb{1} \otimes S_{(j_0,r)})(U \otimes \mathbb{1}), \quad (1)$$

with $\mathcal{P} = \mathbb{1} - |rr\rangle\langle rr|$. If this operator acts on states where the Rydberg states are not populated, it coincides with $C_U(j_0)$. That is, U is applied to the target qudit *if and only if* the control qudit was in state $|j_0\rangle$. The execution time of this gate is upper bounded by $(6d(d-1)+2)T$.

In summary, we have established a gate set $\mathcal{G} = \{U, C_U(j_0)\}$ consisting of arbitrary single-qudit gates $U \in SU(d)$ and the corresponding controlled two-qudit gates $C_U(j_0) \in SU(d^2)$ for any j_0 . These are naturally available in a qudit register consisting of multi-level Rydberg atoms in a programmable tweezer array. The universal properties of \mathcal{G} for general qudit-based algorithms will be discussed elsewhere [77]; here we are specifically interested in the simulation of LGTs as discussed in the following section.

Before continuing, let us briefly pause and discuss possible error sources. We emphasize that our protocols involve excited states $|e\rangle$ and $|r\rangle$ with decay rates $\gamma_{e/r}$. Here we focus on the error caused by a finite value of γ_e . We note that, since $|e\rangle$ is coupled resonantly to the ground-state manifold, the holonomic implementation provides robustness against decoherence caused by spontaneous decay from such state [Fig. 1(a)]. On the other hand, we impose $\Omega \gg 1/T$ to avoid errors caused by non-adiabatic state transfer. This is illustrated in Fig. 2(c), where we show the simulated error $\epsilon = 1 - \mathcal{F}$ [78] of a single-qudit gate relevant for the simulation of LGTs, as described below. Here \mathcal{F} denotes the average gate fidelity [79]. In our simulation we find that for a given value of γ_e/Ω the error can be minimized by increasing ΩT until a saturation point is reached. This sets a minimum clock speed $1/T$ for the quantum processor that may be increased by allowing for larger holonomic errors. More generally, we expect that both the gate fidelity as well as the clock speed can be further increased using optimal control methods, where other error sources can be taken into account [80].

Gauge field dynamics on a qudit quantum computer.— In this section, we turn our attention to the digital simulation of real-time gauge theory dynamics with qudits. Most importantly, we will show that the architecture outlined above provides exactly those resources which are required to simulate LGTs on a quantum device. To see this, we take the Hamiltonian lattice approach [81]. Given a gauge group G and a hypercubic lattice with N_ℓ links ℓ , we represent the state $|\psi(t)\rangle$ at time t on a so-called G -register [36], $|\psi(t)\rangle = \sum_{\mathbf{g}} \psi_t(\mathbf{g}) |\mathbf{g}\rangle$, with $|\mathbf{g}\rangle = |g_1\rangle_1 \otimes |g_2\rangle_2 \otimes \cdots = \bigotimes_{\ell} |g_\ell\rangle_\ell$. Here, every $|g\rangle$ denotes a state labelled by a group element $g \in G$, and the set $\{|g\rangle\}$ forms an orthonormal basis of the local (link) \mathcal{H}_G . Hilbert space For the relevant cases of $G = U(1)$ or $SU(N)$, where \mathcal{H}_G is infinite-dimensional, we replace

G with a large, but finite subgroup of itself, which leads to $\mathcal{H}_G \simeq \mathbb{C}^{|G|}$, with dimension given by the order of the group $|G|$, and thus effectively digitizes the many-body wave-function $\psi_t(\mathbf{g})$ [37]. The state $|\psi(t)\rangle$ can then be encoded naturally in a set of N_ℓ qudits by identifying the computational basis $\{|j\rangle\}$ ($j = 0, \dots, d-1$) with the group state basis $\{|g\rangle\}$ ($g \in G$), with $|G| = d$ [Fig. 1(a)].

The main target of this letter is the time-evolution operator $\mathcal{U}_G(t) = e^{-iH_G t}$ acting on a given initial state $|\psi(0)\rangle$, i.e. we aim to realize the evolution $|\psi(t)\rangle = \mathcal{U}(t)|\psi(0)\rangle$ in a *hardware-efficient* way. For a general Kogut-Susskind-type LGT, this evolution is generated by a Hamiltonian $H_G = \lambda_E H_E + \lambda_B H_B$ with “electric” (E) and “magnetic” contributions (B) [81],

$$H_E = \frac{1}{2} \sum_{\ell} E_{\ell}^2, \quad H_B = \sum_{\square} (\mathcal{U}_{\square} + \mathcal{U}_{\square}^\dagger). \quad (2)$$

While the operator E_{ℓ}^2 acts non-trivially only on a single link ℓ , the plaquette operator

$$\mathcal{U}_{\square} = \text{tr} \left[U_{\ell_1} U_{\ell_2} U_{\ell_3}^\dagger U_{\ell_4}^\dagger \right] \quad (3)$$

involves the four links ℓ_i with $i = 1, \dots, 4$ of an elementary plaquette \square (Fig. 1(b)). To simplify notation we omit here and in the following the links on which \mathcal{U}_{\square} is acting on. For $SU(N)$, the U_{ℓ} are $N \times N$ matrices of operators ($N = 1$ for $U(1)$), and $\text{tr}[\dots]$ denotes the corresponding trace in N dimensions [81].

We now identify the common challenges in realizing $\mathcal{U}^{(G)}(t)$ for an arbitrary (finite) group G . In our digital approach, we employ a Trotter decomposition with step size δt [82] and error of desired order $\mathcal{O}(\delta t^k)$ [83]. This reduces the task to realizing the elementary Trotter steps $\mathcal{U}^{(E/B)}(\delta t) = e^{-i\lambda_{E/B} H_{E/B} \delta t}$, as e.g. $\mathcal{U}^{(G)}(t) = (\mathcal{U}^{(E)}(\delta t) \mathcal{U}^{(B)}(\delta t))^{t/\delta t} + \mathcal{O}(\delta t)$ for a first order decomposition. Note that due to the locality of the interactions these steps can be applied in parallel using the local gates $\mathcal{U}_{\ell}^{(E)}(\delta t) = e^{-i\lambda_E E_{\ell}^2 \delta t}$ and $\mathcal{U}_{\square}^{(B)}(\delta t) = e^{-i\lambda_B (\mathcal{U}_{\square} + \mathcal{U}_{\square}^\dagger) \delta t}$. For any group G , the local gates are given by

$$\mathcal{U}_{\ell}^{(E)}(\delta t) = \sum_{h_{\ell}, g_{\ell} \in G} f^{(E)}(h_{\ell}, g_{\ell}, \delta t) \times |g_{\ell}\rangle_{\ell} \langle h_{\ell}|, \quad (4)$$

$$\mathcal{U}_{\square}^{(B)}(\delta t) = \sum_{g_{\ell_1, 2, 3, 4} \in G} f^{(B)}(g_{\ell_1} g_{\ell_2} g_{\ell_3}^{-1} g_{\ell_4}^{-1}, \delta t) \times |g_{\ell_1}, g_{\ell_2}, g_{\ell_3}, g_{\ell_4}\rangle \langle g_{\ell_1}, g_{\ell_2}, g_{\ell_3}, g_{\ell_4}|, \quad (5)$$

acting trivially on all other links. The group-dependence is encoded in the functions $f^{(E/B)}$ (see SM [76] for explicit expressions). Hence, for $|G| = d$, $\mathcal{U}_{\ell}^{(E)}$ corresponds to a single-qudit gate acting on link ℓ while $\mathcal{U}_{\square}^{(B)}$ represents a diagonal four-qudit gate (acting on links ℓ_1, \dots, ℓ_4).

Let us now decompose the four-qudit diagonal gate, $\mathcal{U}_{\square}^{(B)}$ into more elementary gates [28]. We define the two-qudit gate $\Theta_{\ell|\ell'}$, which realizes a controlled group

multiplication, by $\Theta_{\ell|\ell'}|g_{\ell'}\rangle = |g_{\ell}g_{\ell'}\rangle|g_{\ell'}\rangle$. As $f^{(B)}$ depends only on the product $g_{\ell_1}g_{\ell_2}g_{\ell_3}^{-1}g_{\ell_4}^{-1} \in G$, $\mathcal{U}_{\square}^{(B)}$ can be implemented by applying $\Theta_{\ell|\ell'}^{(\dagger)}$ between link ℓ_1 and the other three links followed by the diagonal single-qudit gate $\mathcal{U}_{\ell}^{(B)}(\delta t)|g_{\ell}\rangle = f^{(B)}(g_{\ell}, \delta t)|g_{\ell}\rangle$, and finally undoing the first operations [Fig. 1(b)]. More explicitly,

$$\mathcal{U}_{\square}^{(B)} = \Theta_{\ell_1|\ell_2}^{\dagger} \Theta_{\ell_1|\ell_3} \Theta_{\ell_1|\ell_4} \mathcal{U}_{\ell_1}^{(B)} \Theta_{\ell_1|\ell_4}^{\dagger} \Theta_{\ell_1|\ell_3}^{\dagger} \Theta_{\ell_1|\ell_2} \cdot \quad (6)$$

In summary, it is sufficient to realize the single-qudit gates $\mathcal{U}_{\ell}^{(E/B)}$ and the two-qudit gate $\Theta_{\ell|\ell'}$ for quantum simulating the real-time dynamics of an arbitrary gauge theory. The latter can be further decomposed into a product of controlled-permutation gates [Fig. 1(a)],

$$\Theta_{\ell|\ell'} = \sum_{g \in G} \theta_{\ell}(g) \otimes |g\rangle_{\ell'} \langle g| = \prod_{g \in G} C_{\theta(g)}^{\ell' \rightarrow \ell}(g). \quad (7)$$

Here, $\ell(\ell')$ denotes the control (target) qudit and $\theta_{\ell}(g)$ is a single-qudit gate implementing the right group multiplication, i.e. $\theta_{\ell}(g)|g_{\ell}\rangle = |g_{\ell}g\rangle$, which is just a permutation. This shows that the required gate set reduces to $\{\mathcal{U}_{\ell}^{(E/B)}, C_{\theta(g)}^{\ell' \rightarrow \ell}(g)\}$, which are precisely the types of gates that are naturally available with the architecture introduced in the previous section. In the spirit of co-design, we have thus identified purpose-made hardware for the digital quantum simulation of LGTs, which is the central result of this letter. Moreover, the possibility of moving the qudits with a programmable tweezer array allows us to perform the required entangling gates in parallel (for example at all even/odd plaquettes in 2D) while avoiding cross-talk from the Rydberg interaction [Fig. 1(a)], making our protocol scalable in system size.

Real-time dynamics of $Q_8 \subset SU(2)$.— To be explicit, we now illustrate our approach for the example of the quaternion group Q_8 , which is the smallest non-abelian subgroup of $SU(2)$ and requires qudits of size $d = 8$ [76]. Using the protocol and hardware described above, the time required to execute a single Trotter step is of the order $\mathcal{O}(10^3)T$, where we used the structure of the group permutation matrices to reduce the number of pulses required to implement $\Theta_{\ell|\ell'}$ to $2(2d-1)(d-1)$ [76]. Fig. 1(c) shows Trotter quench dynamics in comparison to the exact result on a single plaquette, demonstrating that the expected interchange between magnetic and electric energies can be observed with a few tens of Trotter steps. We will next quantify and discuss potential sources of errors which are included in this simulation.

In general, one may distinguish systematic errors due to a finite Trotter step size from errors arising from an imperfect implementation of the individual gates. In our simulations [Fig. 1(c)], we have taken into account an example of the latter in terms of a two-qudit gate $\Theta_{\ell|\ell'}$ with coherent control errors arising from a pulse sequence that is not perfectly adiabatic. To quantify the corresponding error, we calculate the state fidelity of a maximally-entangled state, $|\psi_1\rangle = 1/\sqrt{d} \sum_g |g\rangle |g\rangle$, prepared from a

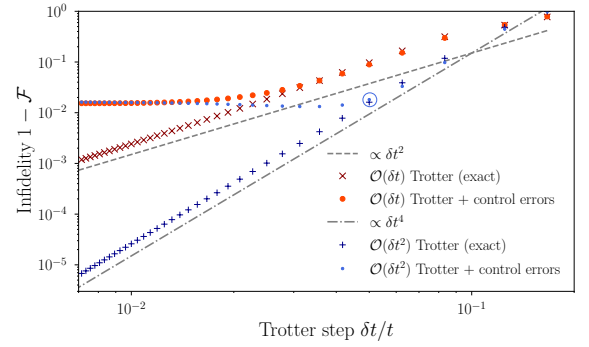


FIG. 3. Fidelity of a Trotter step: The infidelity $1 - \mathcal{F}$ of the digital simulation is controlled by the Trotter step δt . For exact Trotter gates (crosses), the first (second) order decomposition results in the scaling $1 - \mathcal{F} \sim \delta t^{2(4)}$ (dashed/dotted lines). Including control errors of the group-multiplication gate $\Theta_{\ell|\ell'}$, the infidelity saturates at $1 - \mathcal{F} \gtrsim 1\%$ for small δt . The time evolution shown in Fig. 1(c) corresponds to the “sweet spot” of the second-order decomposition including control errors, as indicated by the blue circle.

product state $|\psi_0\rangle = 1/\sqrt{d} \sum_g |0\rangle |g\rangle$ with $|\psi_1\rangle = \Theta |\psi_0\rangle$ [see Fig. 2(d)]. Choosing $\Omega T \approx 300$ and $V/\Omega \approx 5$, we find a small gate error of $\epsilon \sim \mathcal{O}(10^{-4})$. For $\Omega = 2\pi \times 50$ MHz and $V = 2\pi \times 250$ MHz, this leads to a Trotter step time of $\mathcal{O}(1)$ ms, allowing to simulate tens or hundreds of steps within typical experimental coherence times.

For a fixed simulation time t , the Trotter error can be systematically reduced by decreasing δt . At small δt , however, gate errors accumulate, which raises the question how to choose the Trotter step in a given experimental setup. To address this issue, we quantify the overall accuracy of the simulated quantum computation in Fig. 3, where we plot the infidelity $1 - \mathcal{F}$ of the evolution as a function of the Trotter step δt for $t\lambda_B \approx 4.17$. Here, we compare exact simulations of a first (second) order Trotter decomposition to a simulation including coherent control errors arising from the simulated imperfect group-multiplication gate [Fig. 2(d)]. We quantify the accuracy with the overlap of the simulated state (Trotter evolved) $|\psi_{\text{sim}}\rangle$ with the exact result $|\psi_{\text{exact}}\rangle$, i.e. $\mathcal{F} = |\langle \psi_{\text{sim}} | \psi_{\text{exact}} \rangle|^2$. While the observed power-laws clearly show the proper convergence of the Trotter expansion, we find a saturation of \mathcal{F} at small δt when control errors accumulate. It is thus optimal to choose the Trotter step as indicated in Fig. 3, which leads to a high overall accuracy while minimizing the execution time of the simulation.

For small building blocks, like the one-plaquette example considered here, where the exact state $|\psi_{\text{exact}}\rangle$ is available classically, this optimization can be performed by measuring $\mathcal{F}(\delta t)$, which is experimentally accessible through, e.g., the randomized measurement toolbox [84]. More generally, one can efficiently characterize individual Trotter blocks $\mathcal{U}(\delta t) = e^{-iH_F(\delta t)\delta t}$ by measuring the effective Floquet Hamiltonian $H_F(\delta t)$, order by order in δt ,

using a recently proposed protocol based on Hamiltonian learning [85]. Learning the operator content of the error $H_F(\delta t) - H_G$ provides a quantitative estimate of the error of the experimentally implemented Hamiltonian. Moreover, the underlying protocol can be extended to characterize incoherent processes via Liouvillian learning [85], leading to an efficient process tomography that enables a verification of the digital simulation. A detailed study of such a characterization of Trotter blocks, and thus verification of DQS of LGT in the present approach will be presented elsewhere [86].

Conclusions and outlook.— A prerequisite to quantum simulation of non-Abelian LGTs with NISQ devices is hardware efficient encoding and processing with tailored, and scalable quantum hardware. The present work proposes a qudit-based architecture based on atoms stored in tweezer arrays, where single-qudit and entangling gates arising natively in qudit Rydberg-platforms are precisely

those required for the simulation of LGTs, leading to a reduction of the corresponding circuit depth. The present work can be extended to include dynamical matter [87], a necessary step towards addressing open questions in and beyond the Standard Model with quantum simulators.

Acknowledgements.— We thank L. Pastori, H. Pichler, T. Olsacher, R. van Bijnen and E. Zohar for valuable discussions. This work was supported by the US Air Force Office of Scientific Research (AFOSR) via IOE Grant No. FA9550-19-1-7044 LASCEM, the European Union's Horizon 2020 research and innovation program under Grant Agreement No. 817482 (PASQuanS), and by the Simons Collaboration on Ultra-Quantum Matter, which is a grant from the Simons Foundation (651440, P.Z.). JC and BK are grateful for the support of the Austrian Science Fund (FWF): stand alone project P32273-N27 and the SFB BeyondC F 7107-N38.

-
- [1] S. Weinberg, *The quantum theory of fields*, Vol. 2 (Cambridge university press, 1995).
 - [2] I. Montvay and G. Münster, *Quantum fields on a lattice* (Cambridge University Press, 1997).
 - [3] S. Aoki, Y. Aoki, D. Bečirević, T. Blum, G. Colangelo, S. Collins, M. Della Morte, P. Dimopoulos, S. Dürr, H. Fukaya, M. Golterman, S. Gottlieb, R. Gupta, S. Hashimoto, U. M. Heller, G. Herdoiza, R. Horsley, A. Jüttner, T. Kaneko, C. J. D. Lin, E. Lunghi, R. Mawhinney, A. Nicholson, T. Onogi, C. Pena, A. Portelli, A. Ramos, S. R. Sharpe, J. N. Simone, S. Simula, R. Sommer, R. Van de Water, A. Vladikas, U. Wenger, and H. Wittig, Flag review 2019, *The European Physical Journal C* **80**, 113 (2020).
 - [4] M. Troyer and U.-J. Wiese, Computational complexity and fundamental limitations to fermionic quantum monte carlo simulations, *Phys. Rev. Lett.* **94**, 170201 (2005).
 - [5] N. Brambilla, S. Eidelman, P. Foka, S. Gardner, A. S. Kronfeld, M. G. Alford, R. Alkofer, M. Butenschoen, T. D. Cohen, J. Erdmenger, L. Fabbietti, M. Faber, J. L. Goity, B. Ketzer, H. W. Lin, F. J. Llanes-Estrada, H. B. Meyer, P. Pakhlov, E. Pallante, M. I. Polikarpov, H. Sazdjian, A. Schmitt, W. M. Snow, A. Vairo, R. Vogt, A. Vuorinen, H. Wittig, P. Arnold, P. Christakoglou, P. Di Nezza, Z. Fodor, X. Garcia i Tormo, R. Höllwieser, M. A. Janik, A. Kalweit, D. Keane, E. Kiritsis, A. Mischke, R. Mizuk, G. Odyniec, K. Papadodimas, A. Pich, R. Pittau, J. W. Qiu, G. Ricciardi, C. A. Salgado, K. Schwenzer, N. G. Stefanis, G. M. von Hippel, and V. I. Zakharov, Qcd and strongly coupled gauge theories: challenges and perspectives, *The European Physical Journal C* **74**, 2981 (2014).
 - [6] J. Berges, M. P. Heller, A. Mazeliauskas, and R. Venugopalan, Qcd thermalization: Ab initio approaches and interdisciplinary connections, *Reviews of Modern Physics* **93**, 035003 (2021).
 - [7] R. P. Feynman, Simulating physics with computers, *International Journal of Theoretical Physics* **21**, 467 (1981).
 - [8] U.-J. Wiese, Ultracold quantum gases and lattice systems: quantum simulation of lattice gauge theories, *Annalen der Physik* **525**, 777 (2013).
 - [9] E. Zohar, J. I. Cirac, and B. Reznik, Quantum simulations of lattice gauge theories using ultracold atoms in optical lattices, *Reports on Progress in Physics* **79**, 014401 (2015).
 - [10] M. Dalmonte and S. Montangero, Lattice gauge theory simulations in the quantum information era, *Contemporary Physics* **57**, 388 (2016).
 - [11] M. C. Bañuls, R. Blatt, J. Catani, A. Celi, J. I. Cirac, M. Dalmonte, L. Fallani, K. Jansen, M. Lewenstein, S. Montangero, C. A. Muschik, B. Reznik, E. Rico, L. Tagliacozzo, K. Van Acoleyen, F. Verstraete, U.-J. Wiese, M. Wingate, J. Zakrzewski, and P. Zoller, Simulating lattice gauge theories within quantum technologies, *The European Physical Journal D* **74**, 165 (2020).
 - [12] M. Aidelsburger, L. Barbiero, A. Bermudez, T. Chanda, A. Dauphin, D. González-Cuadra, P. R. Grzybowski, S. Hands, F. Jendrzejewski, J. Jünemann, G. Juzeliūnas, V. Kasper, A. Piga, S.-J. Ran, M. Rizzi, G. Sierra, L. Tagliacozzo, E. Tirrito, T. V. Zache, J. Zakrzewski, E. Zohar, and M. Lewenstein, Cold atoms meet lattice gauge theory, *Philosophical Transactions of the Royal Society A: Mathematical, Physical and Engineering Sciences* **380**, 20210064 (2022).
 - [13] E. Zohar, Quantum simulation of lattice gauge theories in more than one space dimension—requirements, challenges and methods, *Philosophical Transactions of the Royal Society A: Mathematical, Physical and Engineering Sciences* **380**, 20210069 (2022).
 - [14] E. A. Martinez, C. A. Muschik, P. Schindler, D. Nigg, A. Erhard, M. Heyl, P. Hauke, M. Dalmonte, T. Monz, P. Zoller, and R. Blatt, Real-time dynamics of lattice gauge theories with a few-qubit quantum computer, *Nature* **534**, 516 (2016).
 - [15] C. Schweizer, F. Grusdt, M. Berngruber, L. Barbiero, E. Demler, N. Goldman, I. Bloch, and M. Aidelsburger, Floquet approach to \mathbb{Z}_2 lattice gauge theories with ultracold atoms in optical lattices, *Nature Physics* **15**, 1168 (2019).

- (2019).
- [16] C. Kokail, C. Maier, R. van Bijnen, T. Brydges, M. K. Joshi, P. Jurcevic, C. A. Muschik, P. Silvi, R. Blatt, C. F. Roos, and P. Zoller, Self-verifying variational quantum simulation of lattice models, *Nature* **569**, 355 (2019).
 - [17] A. Mil, T. V. Zache, A. Hegde, A. Xia, R. P. Bhatt, M. K. Oberthaler, P. Hauke, J. Berges, and F. Jendrzejewski, A scalable realization of local $u(1)$ gauge invariance in cold atomic mixtures, *Science* **367**, 1128 (2020).
 - [18] B. Yang, H. Sun, R. Ott, H.-Y. Wang, T. V. Zache, J. C. Halimeh, Z.-S. Yuan, P. Hauke, and J.-W. Pan, Observation of gauge invariance in a 71-site bose-hubbard quantum simulator, *Nature* **587**, 392 (2020).
 - [19] Z.-Y. Zhou, G.-X. Su, J. C. Halimeh, R. Ott, H. Sun, P. Hauke, B. Yang, Z.-S. Yuan, J. Berges, and J.-W. Pan, Thermalization dynamics of a gauge theory on a quantum simulator, arXiv e-prints, arXiv:2107.13563 (2021), [arXiv:2107.13563 \[cond-mat.quant-gas\]](#).
 - [20] N. H. Nguyen, M. C. Tran, Y. Zhu, A. M. Green, C. Huerta Alderete, Z. Davoudi, and N. M. Linke, Digital Quantum Simulation of the Schwinger Model and Symmetry Protection with Trapped Ions, arXiv e-prints, arXiv:2112.14262 (2021), [arXiv:2112.14262 \[quant-ph\]](#).
 - [21] N. Klco, A. Roggero, and M. J. Savage, Standard model physics and the digital quantum revolution: thoughts about the interface, Reports on Progress in Physics (2022).
 - [22] C. Muschik, M. Heyl, E. Martinez, T. Monz, P. Schindler, B. Vogell, M. Dalmonde, P. Hauke, R. Blatt, and P. Zoller, $U(1)$ wilson lattice gauge theories in digital quantum simulators, *New Journal of Physics* **19**, 103020 (2017).
 - [23] D. Paulson, L. Dellantonio, J. F. Haase, A. Celi, A. Kan, A. Jena, C. Kokail, R. van Bijnen, K. Jansen, P. Zoller, and C. A. Muschik, Simulating 2d effects in lattice gauge theories on a quantum computer, *PRX Quantum* **2**, 030334 (2021).
 - [24] Z. Davoudi, N. M. Linke, and G. Pagano, Toward simulating quantum field theories with controlled phonon-ion dynamics: A hybrid analog-digital approach, *Phys. Rev. Research* **3**, 043072 (2021).
 - [25] L. Tagliacozzo, A. Celi, P. Orland, M. W. Mitchell, and M. Lewenstein, Simulation of non-abelian gauge theories with optical lattices, *Nature Communications* **4**, 2615 (2013).
 - [26] L. Tagliacozzo, A. Celi, A. Zamora, and M. Lewenstein, Optical abelian lattice gauge theories, *Annals of Physics* **330**, 160 (2013).
 - [27] E. Zohar, A. Farace, B. Reznik, and J. I. Cirac, Digital quantum simulation of F_2 lattice gauge theories with dynamical fermionic matter, *Phys. Rev. Lett.* **118**, 070501 (2017).
 - [28] E. Zohar, A. Farace, B. Reznik, and J. I. Cirac, Digital lattice gauge theories, *Phys. Rev. A* **95**, 023604 (2017).
 - [29] J. Bender, E. Zohar, A. Farace, and J. I. Cirac, Digital quantum simulation of lattice gauge theories in three spatial dimensions, *New Journal of Physics* **20**, 093001 (2018).
 - [30] A. Mezzacapo, E. Rico, C. Sabín, I. L. Egusquiza, L. Lamata, and E. Solano, Non-abelian $su(2)$ lattice gauge theories in superconducting circuits, *Phys. Rev. Lett.* **115**, 240502 (2015).
 - [31] N. Klco, E. F. Dumitrescu, A. J. McCaskey, T. D. Morris, R. C. Pooser, M. Sanz, E. Solano, P. Lougovski, and M. J. Savage, Quantum-classical computation of schwinger model dynamics using quantum computers, *Phys. Rev. A* **98**, 032331 (2018).
 - [32] Y. Y. Atas, J. Zhang, R. Lewis, A. Jahanpour, J. F. Haase, and C. A. Muschik, $Su(2)$ hadrons on a quantum computer via a variational approach, *Nature Communications* **12**, 6499 (2021).
 - [33] T. Armon, S. Ashkenazi, G. García-Moreno, A. González-Tudela, and E. Zohar, Photon-mediated stroboscopic quantum simulation of a F_2 lattice gauge theory, *Phys. Rev. Lett.* **127**, 250501 (2021).
 - [34] J. Preskill, Quantum Computing in the NISQ era and beyond, *Quantum* **2**, 79 (2018).
 - [35] T. Byrnes and Y. Yamamoto, Simulating lattice gauge theories on a quantum computer, *Phys. Rev. A* **73**, 022328 (2006).
 - [36] H. Lamm, S. Lawrence, and Y. Yamauchi (NuQS Collaboration), General methods for digital quantum simulation of gauge theories, *Phys. Rev. D* **100**, 034518 (2019).
 - [37] A. Alexandru, P. F. Bedaque, S. Harmalkar, H. Lamm, S. Lawrence, and N. C. Warrington (NuQS Collaboration), Gluon field digitization for quantum computers, *Phys. Rev. D* **100**, 114501 (2019).
 - [38] Y. Ji, H. Lamm, and S. Zhu (NuQS Collaboration), Gluon field digitization via group space decimation for quantum computers, *Phys. Rev. D* **102**, 114513 (2020).
 - [39] S. V. Mathis, G. Mazzola, and I. Tavernelli, Toward scalable simulations of lattice gauge theories on quantum computers, *Phys. Rev. D* **102**, 094501 (2020).
 - [40] D. B. Kaplan and J. R. Stryker, Gauss's law, duality, and the hamiltonian formulation of $u(1)$ lattice gauge theory, *Phys. Rev. D* **102**, 094515 (2020).
 - [41] R. C. Brower, D. Berenstein, and H. Kawai, Lattice Gauge Theory for a Quantum Computer, arXiv e-prints, arXiv:2002.10028 (2020), [arXiv:2002.10028 \[hep-lat\]](#).
 - [42] A. F. Shaw, P. Lougovski, J. R. Stryker, and N. Wiebe, Quantum Algorithms for Simulating the Lattice Schwinger Model, *Quantum* **4**, 306 (2020).
 - [43] N. Klco, M. J. Savage, and J. R. Stryker, $Su(2)$ non-abelian gauge field theory in one dimension on digital quantum computers, *Phys. Rev. D* **101**, 074512 (2020).
 - [44] A. Ciavarella, N. Klco, and M. J. Savage, Trailhead for quantum simulation of $su(3)$ yang-mills lattice gauge theory in the local multiplet basis, *Phys. Rev. D* **103**, 094501 (2021).
 - [45] A. Alexandru, P. F. Bedaque, R. Brett, and H. Lamm, The spectrum of qubitized QCD: glueballs in a $S(1080)$ gauge theory, arXiv e-prints, arXiv:2112.08482 (2021), [arXiv:2112.08482 \[hep-lat\]](#).
 - [46] J. F. Haase, L. Dellantonio, A. Celi, D. Paulson, A. Kan, K. Jansen, and C. A. Muschik, A resource efficient approach for quantum and classical simulations of gauge theories in particle physics, *Quantum* **5**, 393 (2021).
 - [47] C. W. Bauer and D. M. Grabowska, Efficient Representation for Simulating $U(1)$ Gauge Theories on Digital Quantum Computers at All Values of the Coupling, arXiv e-prints, arXiv:2111.08015 (2021), [arXiv:2111.08015 \[hep-ph\]](#).
 - [48] A. Kan and Y. Nam, Lattice Quantum Chromodynamics and Electrodynamics on a Universal Quantum Computer, arXiv e-prints, arXiv:2107.12769 (2021), [arXiv:2107.12769 \[quant-ph\]](#).
 - [49] Z. Davoudi, I. Raychowdhury, and A. Shaw, Search for efficient formulations for hamiltonian simulation of non-

- abelian lattice gauge theories, *Phys. Rev. D* **104**, 074505 (2021).
- [50] A. M. Kaufman and K.-K. Ni, Quantum science with optical tweezer arrays of ultracold atoms and molecules, *Nature Physics* **17**, 1324 (2021).
- [51] M. Saffman, Quantum computing with atomic qubits and rydberg interactions: progress and challenges, *Journal of Physics B: Atomic, Molecular and Optical Physics* **49**, 202001 (2016).
- [52] L. Henriet, L. Beguin, A. Signoles, T. Lahaye, A. Browaeys, G.-O. Reymond, and C. Jurczak, Quantum computing with neutral atoms, *Quantum* **4**, 327 (2020).
- [53] D. Bluvstein, H. Levine, G. Semeghini, T. T. Wang, S. Ebadi, M. Kalinowski, A. Keesling, N. Maskara, H. Pichler, M. Greiner, V. Vuletić, and M. D. Lukin, A quantum processor based on coherent transport of entangled atom arrays, arXiv e-prints, arXiv:2112.03923 (2021), [arXiv:2112.03923 \[quant-ph\]](#).
- [54] S. R. Cohen and J. D. Thompson, Quantum computing with circular rydberg atoms, *PRX Quantum* **2**, 030322 (2021).
- [55] E. Guardado-Sanchez, B. M. Spar, P. Schauss, R. Belyansky, J. T. Young, P. Bienias, A. V. Gorshkov, T. Iadecola, and W. S. Bakr, Quench dynamics of a fermi gas with strong nonlocal interactions, *Phys. Rev. X* **11**, 021036 (2021).
- [56] I. S. Madjarov, J. P. Covey, A. L. Shaw, J. Choi, A. Kale, A. Cooper, H. Pichler, V. Schkolnik, J. R. Williams, and M. Endres, High-fidelity entanglement and detection of alkaline-earth rydberg atoms, *Nature Physics* **16**, 857 (2020).
- [57] E. J. Gustafson, Prospects for simulating a qudit-based model of $(1+1)$ D scalar qed, *Phys. Rev. D* **103**, 114505 (2021).
- [58] E. Gustafson, Noise Improvements in Quantum Simulations of sQED using Qutrits, arXiv e-prints, arXiv:2201.04546 (2022), [arXiv:2201.04546 \[quant-ph\]](#).
- [59] Y. Wang, Z. Hu, B. C. Sanders, and S. Kais, Qudits and high-dimensional quantum computing, *Frontiers in Physics* **8**, 10.3389/fphy.2020.589504 (2020).
- [60] M. Saffman, T. G. Walker, and K. Mølmer, Quantum information with rydberg atoms, *Rev. Mod. Phys.* **82**, 2313 (2010).
- [61] P. Zanardi and M. Rasetti, Holonomic quantum computation, *Physics Letters A* **264**, 94 (1999).
- [62] E. Sjöqvist, D. M. Tong, L. M. Andersson, B. Hessmo, M. Johansson, and K. Singh, Non-adiabatic holonomic quantum computation, *New Journal of Physics* **14**, 103035 (2012).
- [63] G. F. Xu, J. Zhang, D. M. Tong, E. Sjöqvist, and L. C. Kwek, Nonadiabatic holonomic quantum computation in decoherence-free subspaces, *Phys. Rev. Lett.* **109**, 170501 (2012).
- [64] G. Feng, G. Xu, and G. Long, Experimental realization of nonadiabatic holonomic quantum computation, *Phys. Rev. Lett.* **110**, 190501 (2013).
- [65] Y.-H. Kang, Y.-H. Chen, Z.-C. Shi, B.-H. Huang, J. Song, and Y. Xia, Nonadiabatic holonomic quantum computation using rydberg blockade, *Phys. Rev. A* **97**, 042336 (2018).
- [66] M. Ringbauer, M. Meth, L. Postler, R. Stricker, R. Blatt, P. Schindler, and T. Monz, A universal qudit quantum processor with trapped ions, arXiv e-prints, arXiv:2109.06903 (2021), [arXiv:2109.06903 \[quant-ph\]](#).
- [67] Y. Chi, J. Huang, Z. Zhang, J. Mao, Z. Zhou, X. Chen, C. Zhai, J. Bao, T. Dai, H. Yuan, M. Zhang, D. Dai, B. Tang, Y. Yang, Z. Li, Y. Ding, L. K. Oxenløwe, M. G. Thompson, J. L. O'Brien, Y. Li, Q. Gong, and J. Wang, A programmable qudit-based quantum processor, *Nature Communications* **13**, 1166 (2022).
- [68] H. Levine, A. Keesling, G. Semeghini, A. Omran, T. T. Wang, S. Ebadi, H. Bernien, M. Greiner, V. Vuletić, H. Pichler, and M. D. Lukin, Parallel implementation of high-fidelity multiqubit gates with neutral atoms, *Phys. Rev. Lett.* **123**, 170503 (2019).
- [69] S. Ebadi, T. T. Wang, H. Levine, A. Keesling, G. Semeghini, A. Omran, D. Bluvstein, R. Samajdar, H. Pichler, W. W. Ho, S. Choi, S. Sachdev, M. Greiner, V. Vuletić, and M. D. Lukin, Quantum phases of matter on a 256-atom programmable quantum simulator, *Nature* **595**, 227 (2021).
- [70] P. Scholl, M. Schuler, H. J. Williams, A. A. Eberharter, D. Barredo, K.-N. Schymik, V. Lienhard, L.-P. Henry, T. C. Lang, T. Lahaye, A. M. Läuchli, and A. Browaeys, Quantum simulation of 2d antiferromagnets with hundreds of rydberg atoms, *Nature* **595**, 233 (2021).
- [71] A. W. Young, W. J. Eckner, N. Schine, A. M. Childs, and A. M. Kaufman, Tweezer-programmable 2D quantum walks in a Hubbard-regime lattice, arXiv e-prints, arXiv:2202.01204 (2022), [arXiv:2202.01204 \[quant-ph\]](#).
- [72] A. Trautmann, M. J. Mark, P. Ilzhöfer, H. Edri, A. E. Arach, J. G. Maloberti, C. H. Greene, F. Robicheaux, and F. Ferlaino, Spectroscopy of rydberg states in erbium using electromagnetically induced transparency, *Phys. Rev. Research* **3**, 033165 (2021).
- [73] M. Saffman and K. Mølmer, Scaling the neutral-atom rydberg gate quantum computer by collective encoding in holmium atoms, *Phys. Rev. A* **78**, 012336 (2008).
- [74] J. Hostetter, J. D. Pritchard, J. E. Lawler, and M. Saffman, Measurement of holmium rydberg series through magneto-optical trap depletion spectroscopy, *Phys. Rev. A* **91**, 012507 (2015).
- [75] C.-K. Li, R. Roberts, and X. Yin, Decomposition of unitary matrices and quantum gates, *International Journal of Quantum Information* **11**, 1350015 (2013).
- [76] See the Supplementary Material for further details on the implementation of holonomic gates and the digital quantum simulation of the Q_8 LGT.
- [77] J. Carrasco *et al.*, in preparation (2022).
- [78] We calculate the average gate fidelity using the expression $\mathcal{F} = \frac{1}{d(d+1)} [\text{Tr}(MM^\dagger) + |\text{Tr}(M)|^2]$, with $M = PU^\dagger U_{\text{atom}}P$, where U is the target unitary, U_{atom} is the simulated unitary obtained by solving the time-dependent Schrödinger equation for the full pulse sequence on the $(d+2)$ -level atomic system and P is the projection on the qudit subspace.
- [79] L. H. Pedersen, N. M. Møller, and K. Mølmer, Fidelity of quantum operations, *Physics Letters A* **367**, 47 (2007).
- [80] S. Jandura and G. Pupillo, Time-Optimal Two- and Three-Qubit Gates for Rydberg Atoms, arXiv e-prints, arXiv:2202.00903 (2022), [arXiv:2202.00903 \[quant-ph\]](#).
- [81] J. Kogut and L. Susskind, Hamiltonian formulation of wilson's lattice gauge theories, *Physical Review D* **11**, 395 (1975).
- [82] H. F. Trotter, On the product of semi-groups of operators, *Proceedings of the American Mathematical Society* **10**, 545 (1959).

- [83] N. Hatano and M. Suzuki, Finding exponential product formulas of higher orders, in *Quantum Annealing and Other Optimization Methods*, edited by A. Das and B. K. Chakrabarti (Springer Berlin Heidelberg, Berlin, Heidelberg, 2005) pp. 37–68.
- [84] A. Elben, S. T. Flammia, H.-Y. Huang, R. Kueng, J. Preskill, B. Vermersch, and P. Zoller, The randomized measurement toolbox, arXiv e-prints , arXiv.2203.11374 (2022).
- [85] L. Pastori, T. Olsacher *et al.*, in preparation (2022).
- [86] T. Olsacher *et al.*, in preparation (2022).
- [87] D. González-Cuadra *et al.*, in preparation (2022).

SUPPLEMENTAL MATERIAL TO “QUDIT-BASED QUANTUM SIMULATION OF NON-ABELIAN GAUGE THEORIES WITH RYDBERG ATOMS”

In this Supplementary Material we discuss further details for the holonomic implementation of single-qudit gates and the properties of the quaternion group, including its gauge invariant Hamiltonian and the pulse sequence required to implement the corresponding group-multiplication gate.

1. Holonomic gates

We specify here how to implement general single-qudit holonomic gates, less prone to errors [61], using the experimentally available Hamiltonian introduced below. As discussed in the seminal work [61], the notion of generalized Berry phase (i.e., non-Abelian holonomy) can be used to perform universal quantum computations. The computational space is the d -fold degenerate subspace of a family of Hamiltonians (*dark states*) parametrized by a manifold \mathcal{M} representing the couplings between subsystems. This subspace can be taken to be the degenerate null-space of the family of Hamiltonians to be introduced. Adiabatic closed paths in \mathcal{M} induce special unitary transformations $SU(d)$ in the computational subspace. Here we make this construction explicit by introducing a concrete family of Hamiltonians. Given a target unitary in $SU(d)$, we find a path in terms of Gaussian pulses that implements it.

A general single-qudit operation, $U \in SU(d)$ can be decomposed in terms of at most $d(d-1)/2$ operators acting non-trivially only on two consecutive levels [75]. This is, $U = \prod_k \tilde{U}_k$, with $\tilde{U}_k = \mathbb{1}_{j_k-1} \oplus U_k \oplus \mathbb{1}_{d-j_k-1}$, where $U_k \in SU(2)$ acts on a two-dimensional subspace \mathcal{H}_j spanned by $\{|g_{j_k}\rangle, |g_{j_k+1}\rangle\}$. A general unitary acting on two levels can be performed holonomically with the help of two extra auxiliary atomic levels, $|e_{j_k}\rangle$ and $|p_{j_k}\rangle$ [Fig. 4(a)]. Let us consider the following 4-level atomic Hamiltonian,

$$H_{j_k}(\Omega^{(j_k)}) = \frac{1}{2} |e_{j_k}\rangle \left(\Omega_0^{(j_k)} \langle g_{j_k}| + \Omega_1^{(j_k)} \langle g_{j_k+1}| + \Omega_p^{(j_k)} \langle p_{j_k}| \right) + \text{H.c.}, \quad (8)$$

where $\Omega^{(j_k)} = (\Omega_0^{(j_k)}, \Omega_1^{(j_k)}, \Omega_p^{(j_k)})$ denotes a vector of Rabi frequencies that belongs to the parameter manifold \mathcal{M} of the Hamiltonian. In the following, we drop the index j_k to simplify the notation. At every point $\Omega \in \mathcal{M}$, the eigenstates of $H(\Omega)$ consist of two zero-energy dark states and two states with energies $\pm\Delta(\Omega) = \pm\sqrt{|\Omega|^2}$, where a constant non-zero value of Ω_p guarantees that the gap $\Delta(\Omega)$ remains open. In this situation, one can perform $SU(2)$ operations, $u : \mathcal{H}_j \rightarrow \mathcal{H}_j$, via closed loops in the parameter space, $\gamma_C : [t_0, t_1] \rightarrow \mathcal{M}$, with $\gamma(t_0) = \gamma(t_1)$ [Fig. 4(b)]. More specifically, if the loop is traversed adiabatically, u depends only on the geometric properties of the path and is given by [61]

$$u = \mathbf{P} \exp \left(-i \int_{\gamma_C} \sum_{\mu} A^{\mu} d\Omega_{\mu} \right), \quad (9)$$

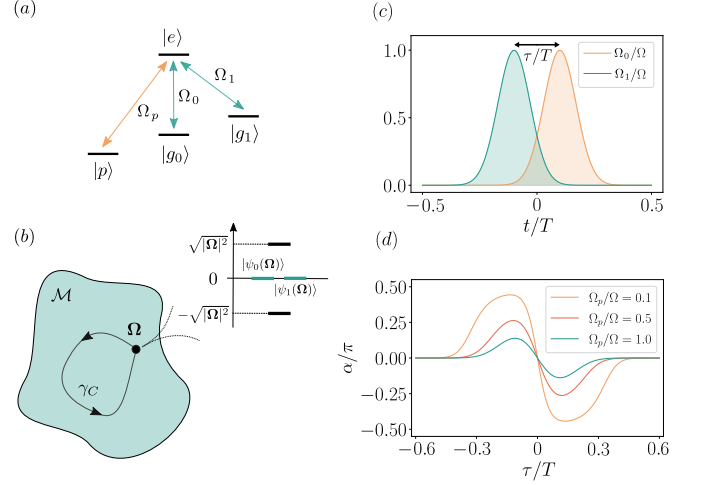


FIG. 4. Single-qudit holonomic gates: (a) Atomic structure used to perform $u \in SU(2)$ operations on \mathcal{H} , a two-level system formed by $|g_0\rangle$ and $|g_1\rangle$. These states, as well as an auxiliary state $|p\rangle$, are coupled to an excited state $|e\rangle$ with laser pulses characterized by the Rabi frequencies $\Omega = (\Omega_0, \Omega_1, \Omega_p) \in \mathcal{M}$. (b) Unitary operations u are performed holonomically in \mathcal{H}_j by adiabatically modifying Ω in \mathcal{M} following close loops γ_C . At every point along the loop, the level structure present two degenerate dark states $\psi_{a=0,1}(\Omega)$ separated from the rest by a gap $\Delta(\Omega)$. (c) Two overlapping Gaussian pulses separated by a time delay τ . (d) Rotation angle α as a function of τ/T for different values of Ω_p/Ω . Note that larger values of α can be reached by applying k consecutive pulses with $\alpha_k = \alpha/k$.

where $(A^{\mu})_{ab} = \langle \psi_a(\Omega) | \partial/\partial\Omega_{\mu} | \psi_b(\Omega) \rangle$ is the connection and $|\psi_{a=0,1}(\Omega)\rangle$ are the corresponding dark states at every point in \mathcal{M} .

By using Gaussian pulses for $\Omega_{a=0,1}$ of the form

$$\Omega_a(t) = \Omega e^{-(t-\tau_a)^2/(T/10)^2} e^{-i\varphi_a} \quad (10)$$

that overlap in time, where T is the pulse time window, and keeping a constant $\Omega_p \neq 0$ to maintain an open energy gap, the following gates are implemented

$$u(\alpha, \delta) = \begin{pmatrix} \cos \alpha & e^{-i\delta} \sin \alpha \\ -e^{i\delta} \sin \alpha & \cos \alpha \end{pmatrix}. \quad (11)$$

Here, $\delta = \varphi_1 - \varphi_0$ is given by the phase difference between the two laser pulses and α depends on its overlap in time, which can be controlled by $\tau = \tau_1 - \tau_0$ [Fig. 4(c)]. The latter can be tuned between $-\pi/2$ and $\pi/2$ by modifying the time delay τ between the pulses [Fig. 4(d)]. In particular, the case $\delta = \pi/2$ (π) corresponds to arbitrary rotations around the X (Y) axis, respectively. Any

SU(2) operation can be written in terms of at most three of these rotations. In summary, any single-qudit operation can be implemented using at most $3d(d-1)/2$ pairs of pulses.

2. The quaternion group Q_8

a. Hamiltonian LGT

In this section, we provide more details about the gauge field digitization via the subgroup $Q_8 \subset \text{SU}(2)$. In particular, the general algorithm employed in the main text requires specific facts about the group multiplication as well as the representation theory of Q_8 , which we summarize below.

The subgroup $Q_8 \subset \text{SU}(2)$ consists of eight elements represented (up to a sign) by the Pauli matrices $\sigma^{x,y,z}$ and the identity matrix σ^0 ,

$$Q_8 = \{\pm\sigma^0, \pm\sigma^x, \pm\sigma^y, \pm\sigma^z\} = \{\pm 1, \pm I, \pm J, \pm K\}. \quad (12)$$

Above we have identified the group elements with the unit quaternions satisfying $I^2 = J^2 = K^2 = IJK = -1$, which explains the common name “quaternion group” for Q_8 . Explicitly, the group multiplication table reads:

	1	-1	I	-I	J	-J	K	-K
1	1	-1	I	-I	J	-J	K	-K
-1	-1	1	-I	I	-J	J	-K	K
I	I	-I	-1	1	K	-K	-J	J
-I	-I	I	1	-1	-K	K	J	-J
J	J	-J	-K	K	-1	1	I	-I
-J	-J	J	K	-K	1	-1	-I	I
K	K	-K	J	-J	-I	I	-1	1
-K	-K	K	-J	J	I	-I	1	-1

The group has five conjugacy classes $\{1\}$, $\{-1\}$, $\{\pm I\}$, $\{\pm J\}$, $\{\pm K\}$ and hence five inequivalent irreducible representations (irreps). These are the trivial irrep **1**, three one-dimensional “alternating” irreps **I**, **J**, **K**, obtained by factoring the normal subgroups generated by I, J, K , respectively, and finally Q_8 inherits the two-dimensional “fundamental” representation **2** from SU(2), which is the only one relevant for our purposes. For completeness, the full character table reads:

χ	$\{1\}$	$\{-1\}$	$\{\pm I\}$	$\{\pm J\}$	$\{\pm K\}$
1	1	1	1	1	1
I	1	1	1	-1	-1
J	1	1	-1	1	-1
K	1	1	-1	-1	1
2	2	-2	0	0	0

In a LGT with gauge group Q_8 , every link carries an eight-dimensional Hilbert space spanned by orthonormal

states $\{|j\rangle\}_{j=1}^8 \equiv \{|\pm 1\rangle, |\pm I\rangle, |\pm J\rangle, |\pm K\rangle\}$. Group multiplication with an element $h \in Q_8$ corresponds, as for any finite group, to a permutation of the group elements. The unitary operator $\theta(h)$ corresponding to the permutation associated to the element $h \in Q_8$ is given by

$$\theta_{g',g}(h) = \langle g' | \theta(h) | g \rangle = \delta_{g',gh}. \quad (13)$$

The corresponding permutation matrix can be directly read off from the group multiplication table. The operators $\theta(g)$ enter the controlled group multiplication gate $\Theta_{\ell|\ell'}$, which we use to implement the plaquette term. The magnetic gate itself further involves the diagonal matrix

$$\mathcal{U}_{g',g}^{(B)} = \langle g' | \mathcal{U}^{(B)} | g \rangle = \delta_{g',g} f^{(B)}(g), \quad (14)$$

where the “magnetic” function $f^{(B)}(g) = e^{-2i\lambda_B \chi^{(2)}(g)\delta t}$ is determined by the character $\chi^{(2)}(g)$ of the irrep **2**. Here, δt denotes the Trotter step size and the coupling $\lambda_B = -\frac{1}{2ag^2}$ is related to the spatial lattice spacing a and the Yang-Mills coupling g^2 . Finally, the electric term is derived from analytic continuation of a transfer matrix of the Euclidean path integral in the standard (Wilson) formulation of SU(2) LGT. Explicitly, the matrix $\mathcal{U}_{g',g}^{(E)} = \langle g' | \mathcal{U}^{(E)} | g \rangle = f^{(E)}(g', g)$ and thus the “electric” function $f^{(E)}$ is implicitly defined by

$$\mathcal{U}^{(E)} = \exp\left(i\delta t \log T^{(E)}\right), \quad T_{g',g}^{(E)} = e^{\frac{2}{\lambda_E a_t} \chi^{(2)}(g'g^{-1})}, \quad (15)$$

where the character is evaluated at the product of the group elements g' and the inverse g^{-1} of g . Here, the coupling $\lambda_E = \frac{g^2}{a}$ is the one from the Kogut-Susskind formulation, but the transfer matrix necessarily involves a finite temporal lattice spacing a_t because no finite subgroup possesses a continuum limit. For the small system discussed in the main text, we have set $a = a_t = 1$ and work with corresponding dimensionless quantities. We conclude this section by noting that Eqs. (13),(14),(15) directly generalize to arbitrary finite subgroups. In the general case, one only needs to replace $2\chi^{(2)} \rightarrow 2\text{Re}[\chi^{(\text{fund.})}]$ with $\chi^{\text{fund.}}$ the character of the fundamental representation of the gauge group of interest and replace the appropriate group-specific details.

b. Pulse sequence

We present here an explicit decomposition of the permutation matrices $\theta(h)$ (see Eq. (13)) corresponding to Q_8 in terms of two-level rotations. Although permutation matrices in SU(d) possess only d non-zero elements, a general decomposition still requires $d(d-1)/2$ two-level unitaries if these are restricted to act between fixed consecutive levels. This is the case for the general encoding of a qudit into d atomic levels belonging to a single

hyperfine manifold, due to the constraints imposed by atomic selection rules to connect different levels. However, an all-to-all connectivity between the different d levels is possible for particular cases if we use different hyperfine manifolds (see Fig. 2 of the main text for an example with $d = 8$). For an all-to-all connectivity, permutation matrices can be then decomposed using only $d - 1$ two-level unitaries which, for the case of Q_8 , correspond to

$$\begin{aligned}
\theta(-1) &= R_{y,2\pi}^{(0,1)} R_{y,\pi}^{(1,2)} R_{y,\pi}^{(2,3)} R_{y,\pi}^{(4,5)} R_{y,2\pi}^{(5,6)} R_{y,\pi}^{(6,7)} , \\
\theta(I) &= R_{y,\pi}^{(0,2)} R_{y,\pi}^{(2,1)} R_{y,\pi}^{(1,3)} R_{y,2\pi}^{(3,4)} R_{y,\pi}^{(6,7)} R_{y,\pi}^{(4,6)} R_{y,\pi}^{(7,5)} , \\
\theta(-I) &= R_{y,\pi}^{(0,3)} R_{y,\pi}^{(3,1)} R_{y,\pi}^{(1,2)} R_{y,2\pi}^{(2,4)} R_{y,\pi}^{(4,6)} R_{y,\pi}^{(6,5)} R_{y,\pi}^{(5,7)} , \\
\theta(J) &= R_{y,\pi}^{(0,4)} R_{y,\pi}^{(4,1)} R_{y,\pi}^{(1,5)} R_{y,2\pi}^{(5,2)} R_{y,\pi}^{(2,6)} R_{y,\pi}^{(6,3)} R_{y,\pi}^{(3,7)} , \\
\theta(-J) &= R_{y,\pi}^{(0,5)} R_{y,\pi}^{(5,1)} R_{y,\pi}^{(1,4)} R_{y,2\pi}^{(4,2)} R_{y,\pi}^{(6,7)} R_{y,\pi}^{(2,6)} R_{y,\pi}^{(7,3)} , \\
\theta(K) &= R_{y,\pi}^{(0,6)} R_{y,\pi}^{(6,1)} R_{y,\pi}^{(1,7)} R_{y,2\pi}^{(7,2)} R_{y,\pi}^{(4,5)} R_{y,\pi}^{(2,4)} R_{y,\pi}^{(5,3)} , \\
\theta(-K) &= R_{y,\pi}^{(0,7)} R_{y,\pi}^{(7,1)} R_{y,\pi}^{(1,6)} R_{y,2\pi}^{(6,2)} R_{y,\pi}^{(2,4)} R_{y,\pi}^{(4,3)} R_{y,\pi}^{(3,5)} .
\end{aligned} \tag{16}$$

This allows us to implement the group-multiplication gate using in total only $2(2d - 1)(d - 1)$ pairs of pulses.